

MASSCLEAN - MASSive CLuster Evolution and ANalysis Package - Description and Tests

Bogdan Popescu and M. M. Hanson

University of Cincinnati, Physics Department, 400 G/P, PO Box 210011, Cincinnati, OH 45221-0011

popescb@email.uc.edu, margaret.hanson@uc.edu

ABSTRACT

We present **MASSCLEAN**, a new, sophisticated and robust stellar cluster image and photometry simulation package. This package is able to create color-magnitude diagrams and standard FITS images in any of the traditional optical and near-infrared bands based on cluster characteristics input by the user, including but not limited to distance, age, mass, radius and extinction. At the limit of very distant, unresolved clusters, we have checked the integrated colors created in **MASSCLEAN** against those from other single stellar population models with consistent results. We have also tested models which provide a reasonable estimate of the field star contamination in images and color-magnitude diagrams. We demonstrate the package by simulating images and color-magnitude diagrams of well known massive Milky Way clusters and compare their appearance to real data. Because the algorithm populates the cluster with a discrete number of tenable stars, it can be used as part of a Monte Carlo Method to derive the probabilistic range of characteristics (integrated colors, for example) consistent with a given cluster mass and age. The discrete nature of our code is demonstrated in the realistic stochastic variation seen in the predicted $V - K$ integrated colors as compared to the unrealistically smooth color from other SSP codes. Our simulation package is available to download and will run on any standard desktop running UNIX/Linux. Full documentation on installation and its use is also available. Finally, a web-based version of **MASSCLEAN** which can be immediately used and is sufficiently adaptable for most applications is available through a web interface.

Submitted to Astronomical Journal

Subject headings: methods: analytical — clusters: general — open clusters and associations: general

1. Introduction

Stellar clusters provide among the most critical observational benchmarks for testing the physics of stellar and galactic evolution and galactic structure. Stellar clusters are easy to exploit because it can be presumed their constituent stars all formed from the same interstellar material (similar initial chemistry) and at the same time (same age). Tinsley (1978) pioneered the application of using stellar evolutionary codes to model the observed characteristics of unresolved stellar clusters and galaxies, referred to as evolutionary population synthesis (Tinsley & Gunn 1976). The present

day version of such methods is seen in the application of *simple stellar population* (hereafter SSP) models to unresolved systems.

Owing to their great utility, a vast array of SSP models have been developed by researchers in the past two decades: Leitherer et al. 1999; Hurley et al. 2000; Schulz et al. 2002; Bruzual & Charlot 2003; Vazquez & Leitherer 2005; Maraston 2005 to name just a few of the most widely used. As these models are applied to a multitude of galactic and extragalactic applications, they each have slightly different techniques in how they include the input physics (beyond differences in which stellar codes they choose). For example, the most

common method derives the emergent properties by integrating along a single stellar isochrone (Charlot & Bruzual 1991), while another technique follows the cluster evolution based on fuel consumption (Maraston 2005). This can lead to perceivable differences in predicted outputs for the same input cluster characteristic (age, metallicity, mass function) from one SSP code to the next, even when the same stellar evolutionary codes are used (see the tests presented in Beasley et al. 2002, Pessev et al. 2008).

Among the variety of SSP codes already available, none have been designed to take advantage of the situation when individual stars are fully or at least partially resolved. The need for a stellar cluster image simulation, based on the tenets of the traditional SSP code, drove us to develop a new analysis tool. Our motivation to develop an image simulation code was to apply it to the search and analysis of deeply embedded massive open clusters lying in the inner Milky Way. However, the code can be applied to Local Group galaxies where massive clusters can be partially resolved with some telescopes.

Our analysis tool, called **MASSCLEAN**, provides image simulations and thus can be used to answer entirely different, important questions in stellar astronomy and galactic structure than previous SSP codes, both within the Galaxy and in nearby external galaxies. In this paper we present the details and current coding of the first release of our new, SSP-like imaging and photometric simulation code, **MASSCLEAN**. In §2, we provide a quantitative description of the computational algorithms used in the routine. In §3 we provide test runs of the simulations comparing the integrated colors and magnitudes against those of currently used SSP codes. We also provide example images with an eye towards accurately modeling well known massive young clusters. In §3.5 and §4, we discuss both the promise and limitations of **MASSCLEAN** for a variety of astrophysical applications.

2. General description of **MASSCLEAN**

Our simulation package, **MASSCLEAN**¹, uses a nominal number of input parameters: mass, initial mass function (hereafter, IMF), metallicity, ex-

inction, distance, spatial distribution parameters and stellar field density. The predicted characteristics are computed for a range of cluster ages from 10^6 to a few 10^9 years. The user can also choose to include a parameter that allows for mass segregation as the cluster ages. Many other features are described in the next sections.

The simulation code is built using numerous well established theoretical and empirical models for stars and stellar clusters, beginning with the Kroupa-Salpeter IMF for mass distribution (Kroupa 2002; Salpeter 1955), the Geneva Models for stellar evolution (Lejeune & Schaerer 2001; Schaller et al. 1992; Schaerer et al. 1993; Charbonnel et al. 1993; Schaerer et al. 1993; Meynet et al. 1994; Charbonnel et al. 1996; Mowlavi et al. 1998; Charbonnel et al. 1999) the extinction model based on Cardelli, Clayton and Mathis 1989, the King Model for spatial distribution (King 1962) and the SKY Model for the stellar field (Wainscoat et al. 1992; Cohen 1994; Cohen 1995; Bahcall & Soneira 1984). This is reviewed in more detail below.

It was our intent to make **MASSCLEAN** user friendly and versatile. The package is designed to allow the user significant latitude and flexibility in how they will apply it. **MASSCLEAN** is written as a series of independently run sub-routines, performing individual calculations at various stages. This allows users to substitute their own inputs at any stage or to skip or perform their own calculations in lieu of those provided within the **MASSCLEAN** package. Information is passed from one routine to the next through read/write of ASCII files. While these files become quite large (gigabyte is not uncommon for the entire output of hundred of files), this allows users of the **MASSCLEAN** routines to easily check, edit and or substitute the output at any stage in the calculations. Although it can take some time to generate images, the code for the photometric simulation is very fast. The package is freely available under GNU General Public License at <http://www.physics.uc.edu/~bogdan/>. Downloadable documentation on installing and running the code is also available. Finally, **MASSCLEAN.web**, a web-based interface, is immediately available² and can be used for many basic applications.

¹ **MASSCLEAN** (**MASS**ive **CL**uster **E**volution and **AN**alysis) package

² <http://www.physics.uc.edu/~bogdan/massclean/>

2.1. The Mass Distribution

The number of stars formed in the $(M, M+dM)$ range is:

$$dN = \xi(M)dM \quad (1)$$

The multi-part power law $\xi(M)$ derived from Kroupa-Salpeter IMF (Kroupa 2002; Salpeter 1955) is :

$$\xi(M) = k \begin{cases} \left(\frac{M}{m_1}\right)^{-\alpha_1} & , \quad m_0 < M \leq m_1 \\ \left(\frac{M}{m_1}\right)^{-\alpha_2} & , \quad m_1 < M \leq m_2 \\ \left(\frac{m_2}{m_1}\right)^{-\alpha_2} \left(\frac{M}{m_2}\right)^{-\alpha_3} & , \quad m_2 < M \leq m_3 \end{cases} \quad (2)$$

with mass expressed in M_\odot units and :

$$\begin{aligned} \alpha_1 &= +0.3 \pm 0.7 & , & \quad 0.01 \leq M/M_\odot < 0.08 \\ \alpha_2 &= +1.3 \pm 0.5 & , & \quad 0.08 \leq M/M_\odot < 0.50 \\ \alpha_3 &= +2.3 \pm 0.3 & , & \quad 0.50 \leq M/M_\odot < m_3 \end{aligned} \quad (3)$$

and $m_3 = \infty$ or $m_3 = m_{up}$ (for an IMF with upper mass cutoff (Oey & Clarke 2005)). Using $\xi(M)/k = \xi_i(M)$ (with $i = 1, 2, 3$ respectively), the total mass of the cluster can be written :

$$M_{total} = \int_0^{N_{total}} M(N)dN \quad (4)$$

$$M_{total} = \int_{m_0}^{m_3} M \frac{dN}{dM} dM = \int_{m_0}^{m_3} \xi(M) M dM \quad (5)$$

$$M_{total} = \sum_{i=1}^3 \left(k \int_{m_{i-1}}^{m_i} \xi_i(M) M dM \right) \quad (6)$$

The normalization constant :

$$k = \frac{M_{total}}{\sum_{i=1}^3 \left(\int_{m_{i-1}}^{m_i} \xi_i(M) M dM \right)} \quad (7)$$

From the equations (1) and (7) :

$$N_i(M, M+dM) = \frac{M_{total} \int_M^{M+dM} \xi_i(M) dM}{\sum_{i=1}^3 \left(\int_{m_{i-1}}^{m_i} \xi_i(M) M dM \right)} \quad (8)$$

Our package uses equation (8) to compute the mass distribution of stars based on the total mass of the cluster M_{total} and the IMF, described by the three $\xi_i(M)$. The mass range to be included in the distribution is chosen by the user. The values α_i and m_i are also input parameters. In this way, a Kroupa IMF can become a Salpeter IMF when $\alpha_1 = \alpha_2 = \alpha_3 = 2.35$. The versatility of the package allows us to use a first-order, second-order or third-order power law model (Kroupa-Salpeter type) for the IMF. The use of a truncated IMF is optional. All the mass bins $(M, M+dM)$ are computed such that the value of $N_i(M, M+dM)$ is an integer (up to some tolerance, also chosen by the user). The program allows fluctuations in the computed mass distribution, such that the distribution is different for every run. The user can turn this feature on or off.

The characteristics of the stellar mass distribution, whether truncated or tied to the cluster mass, etc., are an important component of a stellar cluster for a variety of investigations. This is why the MASSCLEAN package offers a wide array of options to build the stellar mass distribution. Sample computed mass distributions are presented in Figure 1.

2.2. Evolutionary Models

A variety of evolutionary tracks have been used in simulation codes to define the relationship between age and metallicity and integrated broad-band colors or spectral features (Charlot 1996, Brocato et al. 2000, Bruzual & Charlot 2003, Leitherer et al. 1999). Selecting which models to use in a simulation is influenced by the goals of that simulation. In our case, we are most interested in modeling young and intermediate age clusters ($10^7 < \text{age} < 10^9$ years), hence we chose the Geneva Models (Lejeune & Schaerer 2001). These models provide excellent treatment of the evolutionary properties of high mass stars and ample time sampling to closely follow the evolution of a young cluster (age $\geq 10^7$ years). This is very important, particularly in the study of young clusters where evolution occurs quickly and the light from a few massive stars can dominate the light of the cluster.

Finally, we note that the Geneva isochrones and tracks are presently only the default input to the MASSCLEAN package. The package can easily be

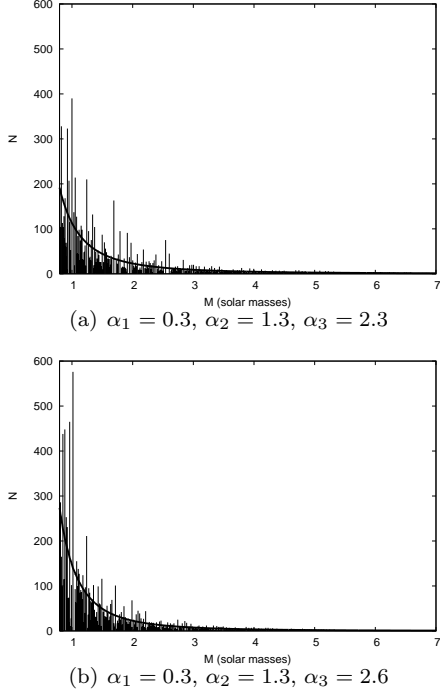


Fig. 1.— Mass distribution for $M_{total} = 5 \times 10^4 M_{\odot}$ using Kroupa IMF. Because all the bins above $7M_{\odot}$ contain only one star, only the $[0.8, 7.0]$ interval is displayed. The solid line shows the mathematical form of the distribution for constant width bins.

switched to use a different set of isochrones and tracks as the user sees fit, such as evolutionary models tailored to old stars, or low metallicity, etc. One can also expand the current set of photometric bands to include the ultraviolet and mid-infrared. Finally, our intention is to provide full compatibility with the new Padova 2008 Database (Marigo et al. 2008) in an update of the code and as soon as the entire set of isochrones and tracks become available.

2.3. CCM Extinction Model

We wish to use our simulations in the study of Milky Way clusters as well as more distant extragalactic clusters and must pay serious attention to extinction effects. For the extinction, the user can enter the value in two ways: the exact extinction value can be entered manually (in the configuration file) for every band or the extinction in each band can be computed using an inputted R_V

and A_V and applying the CCM Extinction Model (Cardelli, Clayton and Mathis, 1989). A sample computed extinction curve is presented in Figure 2.

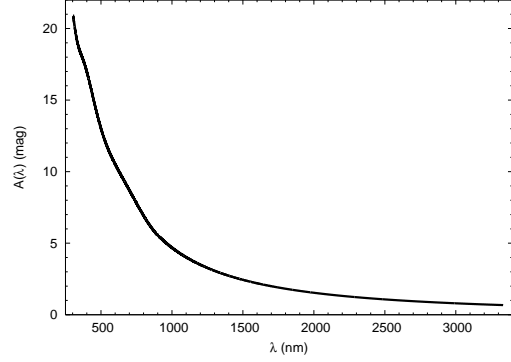


Fig. 2.— CCM Extinction Model, $A_V = 11.6$, $R_V = 3.1$

2.4. Spatial Distribution

Finally, the MASSCLEAN package differs greatly from previous extragalactic SSP codes in that it produces simulated images of the stellar clusters. Thus, the code is concerned with selecting appropriate spatial parameters defined by the angular size (linear scale and distance to the cluster) and for the first time, intrinsic stellar density. To accomplish this we have introduced the King Model Distribution (King 1962), given by :

$$f(r) = k \left[\left(\sqrt{1 + \left(\frac{r}{r_c} \right)^2} \right)^{-1} - \left(\sqrt{1 + \left(\frac{r_t}{r_c} \right)^2} \right)^{-1} \right]^2 \quad (9)$$

An anisotropic spatial distribution can even be generated such that it still obeys the radial King profile. An ellipsoid in a prolate or oblate projection can be generated according to the parameters entered by the user in the configuration file. The rotation angle is also selected by the user.

A simple linear mass segregation feature allows more massive stars to fall toward the cluster's center as the cluster ages (this feature can be turned on or off).

The file containing the spatial distribution can be replaced by another file provided by the user

(based for example on coordinates from a real image).

Sample computed spatial distributions are presented in Figure 3.

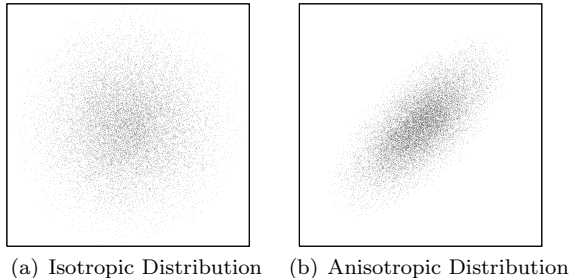


Fig. 3.— King Distribution, $r_c = 0.50$ pc, $r_t = 0.72$ pc, $M_{total} = 10^5 M_\odot$

2.5. Description of the Stellar Field

The MASSCLEAN package has the option to include a field star population. This may be a simulated one, using the SKY Model for the stellar field (Wainscoat et al. 1992; Cohen 1994; Cohen 1995; Bahcall & Soneira 1984) or a real one.

In the first case, starting from the total number of stars brighter than the selected magnitude limit (which is an input parameter), the distribution is generated using the slope of the cumulative numbers of stars (which is also an input parameter), such as shown in Figure 4. Colors are computed based on the Geneva Models (Lejeune & Schaerer 2001) and the *BaSeL*-2.2 grid (Lejeune et al. 1998). Extinction is also included and the user has the option to provide the values for every band. The program used to generate Figure 4 can compute the necessary parameters for a simulated stellar field based on a real one.

The second option is to use a real stellar field. Since the file format is the same as the one used by SKYMAKER (Bertin 2001; Bertin & Fouqué 2007) and SExtractor (Bertin & Arnout 1996), from the computational point of view there is no difference between a real and a simulated stellar field. MASSCLEAN can use a real stellar field provided by SExtractor. The user can also choose not to include any stellar field at all.

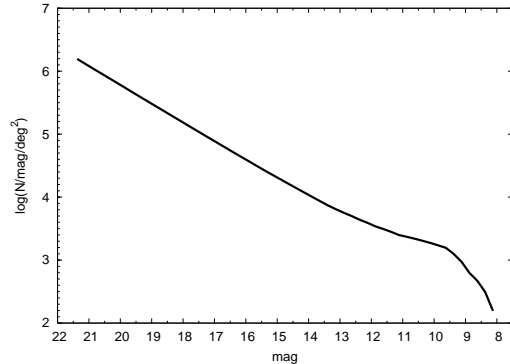


Fig. 4.— Cumulative number of stars vs. magnitude

2.6. Creating the FITS Images and HR Diagrams

Using all of the above models, MASSCLEAN computes actual mass, absolute and apparent magnitude (UBVRIJHK), color indexes, temperature, luminosity and position for all the stars and all the ages included in the Geneva Database (or which ever isochrones one employs). The default age range is $\log(\text{age}/\text{yr}) = 6.0 - 9.5$, but the option to run it only for a few selected values is also available. These outputs are directly used to generate the color-magnitude diagrams and images. There are available relations of transformation from UBVRIJHK to different bandpasses. However, after the addition of the new Padova Models, the bandpasses for HST, 2MASS and Spitzer will be directly available.

The FITS images in each of the broad bands are generated using SKYMAKER (Bertin 2001; Bertin & Fouqué 2007). MASSCLEAN writes all the necessary scripts to run SKYMAKER that generates the images. The configuration files for galactic and extragalactic clusters are also provided, so no knowledge about SKYMAKER is required. The description of the PSF is available in these configuration files and can be changed by the user. In addition to that, SKYMAKER can work with a different PSF provided by the user in a separate file. The users can make any plot from the package's output using the plotting program of their choice, but MASSCLEAN also writes a script which generates HR and color-magnitude diagrams.

3. Tests of the MASSCLEAN Package

Before demonstrating the unique utility of MASSCLEAN and directly comparing its output to real clusters, we will first provide a few logical tests. Our first test will be to derive from MASSCLEAN, the same kind of values which come from other cluster simulation programs which are widely used in the field to ensure that MASSCLEAN gives consistent results. MASSCLEAN does not generate spectral features, such as provided by *Starburst99* (Leitherer et al. 1999). However, it can be made to generate integrated magnitudes and colors. This is achieved by simply summing up the flux over all stars in the final simulated cluster.

3.1. Integrated colors as a function of age and metallicity

The most commonly-used discriminator in the study of extragalactic super cluster studies is integrated colors (Holtzman et al. 1992, Fusi Becci et al. 2005). This is because it is typically the only information obtainable for very distant, unresolved star clusters (Whitmore & Schweizer 1995). Among the most widely-used SSP models for interpreting integrated colors are those given by Bruzual & Charlot (2003) (GALAXEV), and Schulz et al. (2002) and Anders & Fritze – v. Alvensleben (2003) (GALEV). We shall provide a side by side comparison of MASSCLEAN against these two modern SSP codes.

The default age range for MASSCLEAN is [6.0, 9.5] in the logarithmic scale. In Figure 5 (a), (b) and Figure 6 we used a smaller age range in order to accommodate the data from all the available models. In Figure 5 (a) we plot the variation of integrated colors with age for different SSP models. Models using solar metallicity are presented here. The results from MASSCLEAN, shown as the solid line, are compared with GALEV Models in dashed-dotted line, GALAXEV models using Geneva 1994 tracks are shown in the dashed line, and GALAXEV models using Padova 1994 tracks are shown in the dotted line. Specifically, the MASSCLEAN colors follow quite closely to the colors given by GALAXEV with the Geneva 1994 models of Bruzual & Charlot 2003. This was to be expected since the input evolutionary models are essentially identical to those used in MASSCLEAN. The differences between the Padova 1994 based models

and Geneva 1994 models is thoroughly discussed by Bruzual & Charlot 2003. For our purposes, Figure 5 (a) demonstrates that our code, based on a finite stellar generation algorithm, gives the same integrated color results to other codes that use a statistically weighted mass distribution.

However, one does see one very different effect from our integrated colors in the V-K diagram of Figure 5 (a) and (b) : the V-K color varies somewhat erratically in MASSCLEAN compared to the very smooth variation with age seen by the GALAXEV and GALEV models. Although the modern SSP codes can provide very accurate integrated colors for galaxies, we think that they fail to show the real behaviour of a stellar cluster, especially in infrared. The SSP codes randomly populate the entire isochrone for a given age. But real stellar evolution will produce a gap between some of the most luminous stars and the rest, so the isochrones won't be fully populated regardless of the mass of the cluster. This gap is very apparent in the infrared bands, due to the ascendent shape of the tracks in the CMDs. This effect is masked in the visible bands due to the descendent shape of the tracks in CMDs. In the visible bands the gap will be much smaller and the isochrone will appear to be fully populated. This effect appears in the Figure 5 (a) : the U-B and B-V colors are similar to other SSP models, but V-K color is affected by the infrared gap at K. The visible colors are not so sensitive to the total mass of the cluster (also seen in the MASSCLEAN simulations) with this effect becoming more profound as one moves to the infrared bands (see also Cerviño & Luridiana 2006). Additionally, the fluctuation in V-K shown above in the $\log(\text{age}/\text{yr}) = 8$ range will inversely depend on the total mass of the cluster (we used a total mass of $2 \times 10^5 M_\odot$).

The variation of integrated colors with age computed by MASSCLEAN for different metallicity are presented in Figure 5 (b). Again, similarities are seen between the MASSCLEAN predictions and those from programs relying on the same input stellar physics. Overall, bluer, seemingly younger colors are seen with lower metallicity (Schulz et al. 2002; Bruzual & Charlot 2003). The V-K colors in particular, show rather large variations in the first 10^8 years with different input metallicity, Figure 5 (b), similar to that shown in Figure 2 of Bruzual & Charlot 2003.

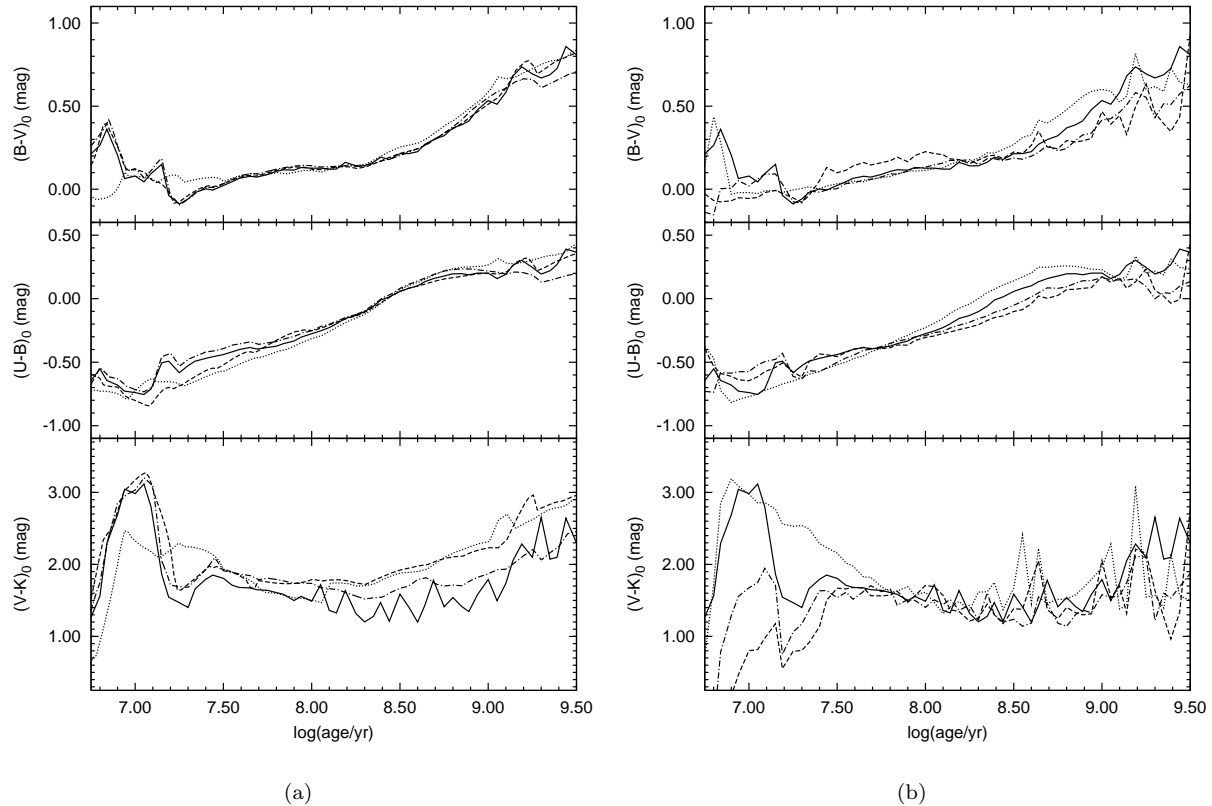


Fig. 5.— (a) Integrated colors for different SSP Models as a function of age for solar metallicity: Geneva 2001 (MASSCLEAN) - solid line; GALEV 2003 - dashed-dotted line; GALAXEV with Geneva 1994 - dashed line; GALAXEV with Padova 1994 - dotted line. (b) Integrated colors for different metallicities as a function of age computed by MASSCLEAN: $Z = 0.020$ (solar) - solid line; $Z = 0.008$ - dashed-dotted line; $Z = 0.004$ - dashed line; $Z = 0.040$ - dotted line.

The variation of integrated colors for different IMFs as computed by MASSCLEAN are presented in Figure 6. Previous studies have noted the very weak sensitivity of the IMF on the integrated colors of stellar clusters over this age range (see, for example, Figure 4 of Bruzual & Charlot 2003).

Finally, in the top panel of Figure 7 we present the evolution of integrated colors $(U - B)_0$ vs $(B - V)_0$ for several different SSP models along side predictions coming from MASSCLEAN (solid line). All simulations were made using solar metallicity. The MASSCLEAN colors continue to compare well with previous work that has been shown to compare well with real data (Girardi et al. 1995). The lower panel shows predicted color evolution

using MASSCLEAN, but showing a variety of metallicities.

3.2. Color-magnitude diagrams

Our next test will be to simulate HR and color-magnitude diagrams of clusters using MASSCLEAN. As a first demonstration, we provide in Figure 8, an HR Diagram for a stellar cluster with a total mass of $10^5 M_\odot$ and a $\log(\text{age}/\text{yr}) = 6.65$. While the individual stars in the cluster are clearly seen at the high mass end, crowding prevents one from seeing anything but a broad blur of stars below about $40 M_\odot$. Naturally, this figure looks no different from the Geneva isochrones used for that same age. In Figure 8(a) the stars have been re-

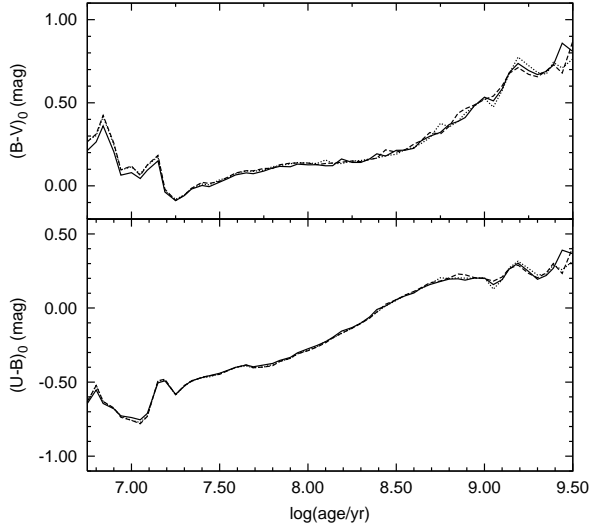


Fig. 6.— Integrated colors for different IMFs as a function of age computed by **MASSCLEAN**: Kroupa IMF $\alpha_3 = 2.6$ - solid line; Kroupa IMF $\alpha_3 = 2.3$ - dashed line; Salpeter IMF - dotted line

binned to take on a more natural range of values; in Figure 8(b) the stars follow a pure single isochrone. We also provide an example of a color-magnitude diagram, V versus $B-V$ for this same simulated cluster, in Figure 9. At the low mass end, again a small variation has been introduced to give the main sequence some width in Figure 9(a). The widening in Figure 8(a) and Figure 9(a) is a user's choice, the maximum width is an input parameter (this option can also be turned on or off) and could be set up to correspond to the photometric error.

The cluster mass and age shown in these two figures was selected explicitly. It matches the estimated mass and age of the Milky Way cluster, *Westerlund 1*. The parameters used for this simulation are based on Westerlund (1961), Clark & Negueruela (2002), Clark et al. (2005) and Figer et al. (2006). We adopted the following values: $M_{total} = 10^5 M_\odot$, solar metallicity, $A_V = 11.6$ mag, $R_V = 3.1$, $r_t = 0.72$ pc and $r_c = 0.50$ pc.

There is a large uncertainty in the distance to *Westerlund 1*. We adopted a distance of $d = 4$ kpc

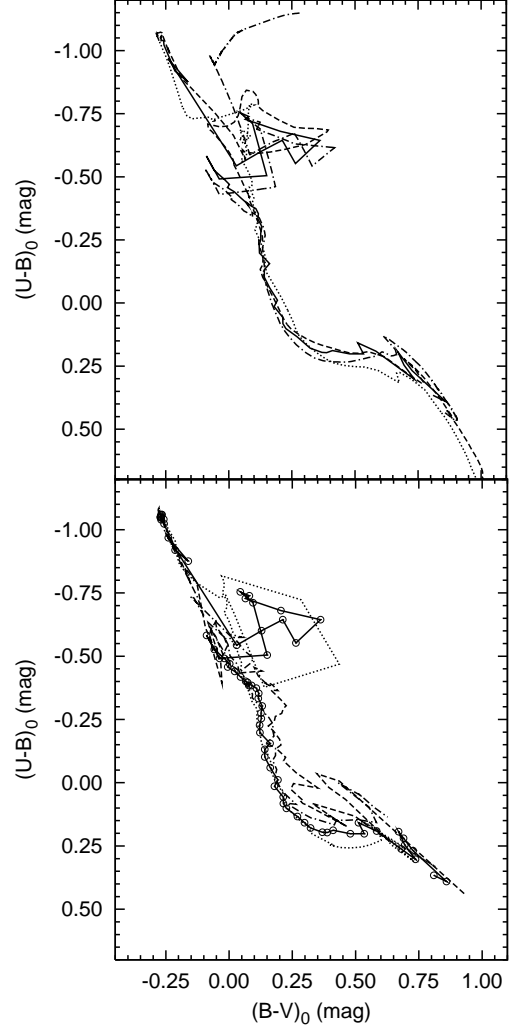


Fig. 7.— Integrated colors $(U - B)_0$ vs $(B - V)_0$. *Upper panel*: Geneva 2001 (**MASSCLEAN**) - solid line; GALEV 2003 - dashed-dotted line; GALAXEV with Geneva 1994 (Bruzual & Charlot) - dashed line; GALAXEV with Padova 1994 (Bruzual & Charlot) - dotted line. *Lower panel*: **MASSCLEAN**: $Z = 0.020$ (solar) - solid line; $Z = 0.008$ - dashed-dotted line; $Z = 0.004$ - dashed line; $Z = 0.040$ - dotted line. The circles along the solar metallicity path correspond to the $\Delta \log(\text{age}/\text{yr}) = 0.05$.

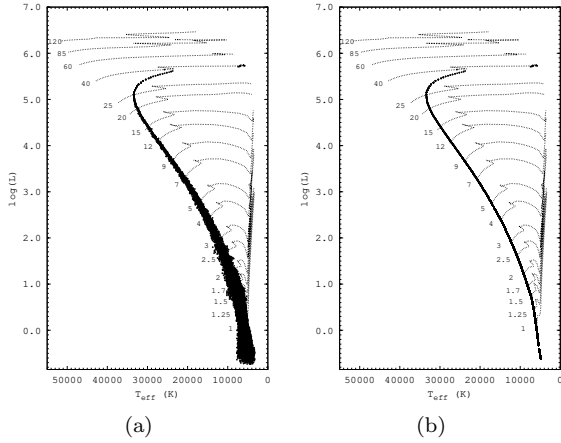


Fig. 8.— MASSCLEAN simulated HR Diagram, for cluster properties $\log(\text{age}) = 6.65$, $M_{\text{total}} = 10^5 M_{\odot}$. In (a), a rebinning has been done to give the stars a more realistic range of values. In (b), one sees the stars following a theoretical track from the Geneva Database. Both figures cover the stellar masses from $120 M_{\odot}$ to $1 M_{\odot}$.

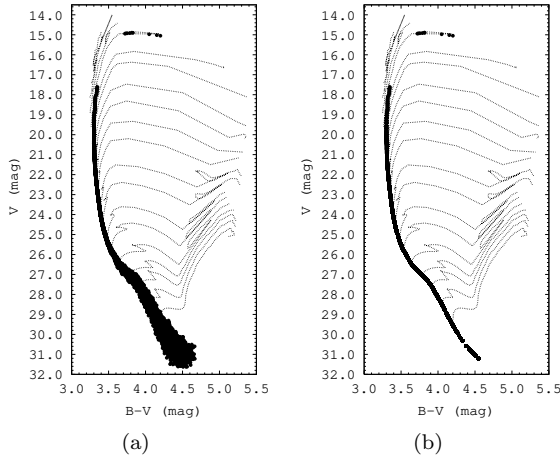


Fig. 9.— The V vs $(B-V)$ color-magnitude diagram, $A_V = 11.6$, $\log(\text{age}) = 6.65$, $M_{\text{total}} = 10^5 M_{\odot}$. The tracks correspond to the same values of mass as in Figure 8.

(distance modulus 13.01 mag). A Kroupa IMF has been used, with $\alpha_1 = 0.3$, $\alpha_2 = 1.3$ and $\alpha_3 = 2.3$. Our simulation shows that the best agreement with the actual data corresponds to the isochrone $\log(\text{age}) = 6.65$. Our results agree with the recent results of Brandner et al. (2008).

In Figure 10 and Figure 11, we present near-infrared color-magnitude diagrams for *Westerlund 1*. MASSCLEAN isochrones (Geneva isochrones, effectively) are overlayed with real photometry for the cluster. We cannot present optical color-magnitude diagrams for this cluster because of the enormous incompleteness due to high extinction ($A_V = 11$). The photometric data in Figure 10 and Figure 11 was taken from the 2MASS and NOMAD (Zacharias et al. 2004) catalogs.

Critical to the utility of MASSCLEAN as a means to constrain the properties of observed clusters, a method for determining the best simulation inputs must still be developed. There is unlikely to be a straightforward way to determine the best fitting simulated image. Rather, we expect comparisons between simulated and real data will need to be done within the CMDs or comparing photometry. This is presently being worked on, but we expect to base such a goodness of fit on observed versus simulated cumulative distribution functions in various photometric bands and using a Kolmogorov-Smirnov test to select the closest fitting simulation (Popescu & Hanson, in prep.).

3.3. Image simulations of Galactic clusters

Our most visual demonstration will be the image simulations provided by MASSCLEAN. The MASSCLEAN package has been used to simulate several well known young Milky Way clusters: *NGC 3603* and *h* and χ *Persei* (*NGC 869*, *NGC 884*), as well as *Westerlund 1*. This correspond to a mass range from $4.3 \times 10^3 M_{\odot}$ to $10^5 M_{\odot}$.

Using the input characteristics given in §3.2, we have created a simulation of *Westerlund 1* in the J-band and provided in Figure 12 (a). This can be compared directly with the 2MASS³(Skrutskie et al. 2006) J-band image of

³ This publication makes use of data products from the Two Micron All Sky Survey, which is a joint project of the University of Massachusetts and the Infrared Processing and Analysis Center/California Institute of Technology, funded by the National Aeronautics and Space Administration and

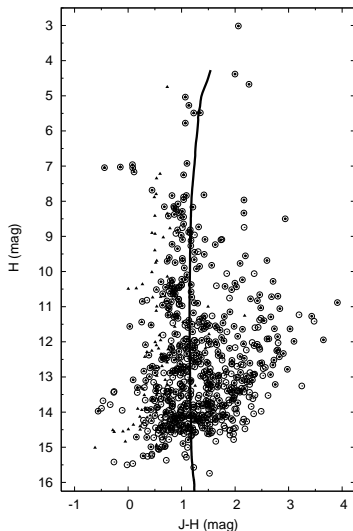


Fig. 10.— H vs. $J - H$ color-magnitude diagram for *Westerlund 1*. Circles - 2MASS source catalog 4.8' radius; dots - 2MASS source catalog 2.0' radius; triangles - NOMAD catalog 4.8' radius. The solid line correspond to the $\log(\text{age}/\text{yr}) = 6.65$ isochrone.

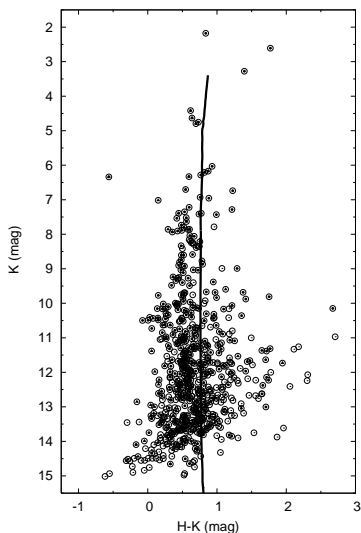


Fig. 11.— K vs. $H - K$ color-magnitude diagram for *Westerlund 1*. Circles - 2MASS source catalog 4.8' radius; dots - 2MASS source catalog 2.0' radius; triangles - NOMAD catalog 4.8' radius. The solid line correspond to the $\log(\text{age}/\text{yr}) = 6.65$ isochrone.

Westerlund 1 shown as Figure 12 (b). In looking at this comparison, one might also consider Figs. 9(a) and 10(a). Presently, the simulated image has a non-realistic 'flatness' in the stellar brightnesses due to several RSGs clustered with a very similar magnitude and color. Some amount of rebinning to randomize slightly the properties of the RSGs (something the cluster will have done more naturally with the non-zero cluster age distribution) may be desirable to include in future updates and releases of the code.

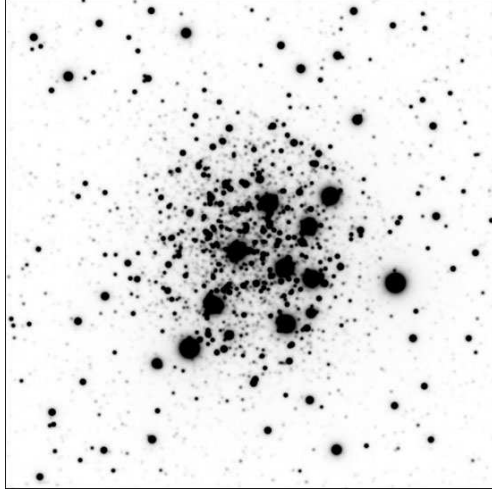
Using the data from Stolte et al. (2004) and Stolte et al. (2006) we simulated *NGC 3603* using: $\log(\text{age}) = 6.00$, $M_{\text{total}} = 10^4 M_{\odot}$ and solar metallicity, $A_V = 4.5$ mag, $R_V = 3.1$, distance $d = 6$ kpc (distance modulus 13.9 mag). For the spatial distribution we used $r_t = 4.4'$ and $r_c = 0.4'$. We note that a single-power Salpeter IMF could not lead to an agreement with the actual photometric data. The best fit corresponds to Kroupa IMF with $\alpha_1 = 0.3$, $\alpha_2 = 1.3$ and $\alpha_3 = 2.4$. The J-band image is shown in Figure 13(a), and the 2MASS (Skrutskie et al. 2006) image is shown in Figure 13(b). It should be clear to the reader we do not include nebulosity in the image simulations.

We have built a suite of different cluster models by varying all of the input variables within the range of known measurements for these two clusters. These resulting simulations were tested against the available catalogs of images and photometric data for the two clusters. A complete analysis for *NGC 3603* and *Westerlund 1* will be presented in a subsequent paper, along with the development of a proper goodness of fit (Popescu & Hanson, in prep.).

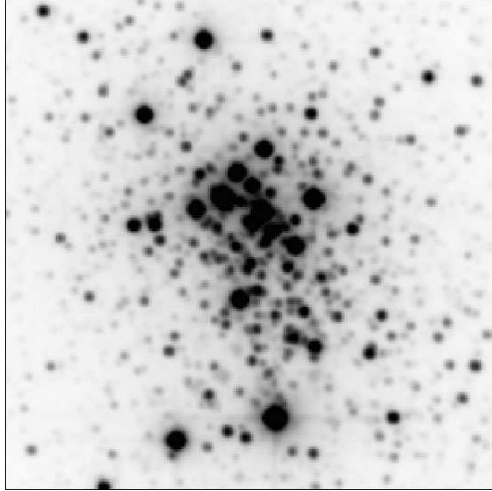
3.4. Simulations of multiple starburst events or subclustering

MASSCLEAN can be used to simulate clusters with multiple starbursting events. As a demonstration of this, we present the twin cluster *h* and χ *Persei* (*NGC 869*, *NGC 884*), simulated based on measurements made by Bragg (2004). Our V-band simulation is shown in Figure 14. Here, we applied the following inputs to our simulation: $\log(\text{age}_h) = 7.05$, $\log(\text{age}_\chi) = 7.09$, $M_h = 5.5 \times 10^3 M_{\odot}$, $M_\chi = 4.3 \times 10^3 M_{\odot}$. For both clusters we assumed solar metallicity, $A_V = 1.6$

the National Science Foundation.

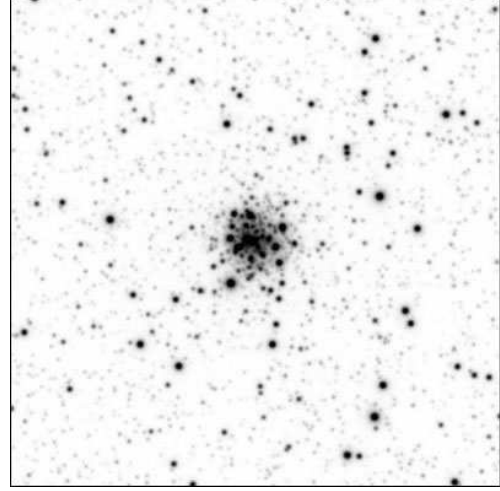


(a) Simulated Image

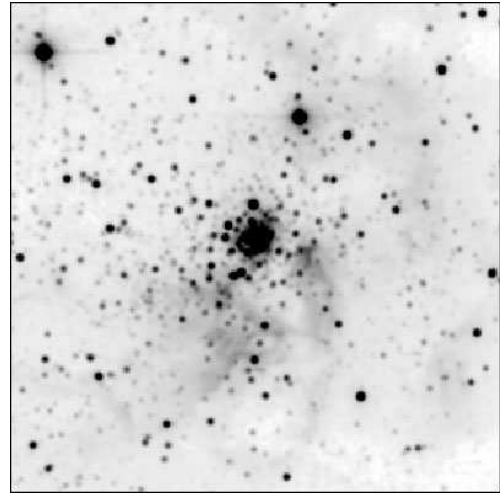


(b) 2MASS Image

Fig. 12.— MASSCLEAN simulated images of *Westerlund 1*. In the upper panel (a) we provide the simulated image in the *J* Band. A simulated field star population has been included. The lower panel comes from 2MASS and is also in the *J* Band. Both fields shown are for a $4.8' \times 4.8'$ image.



(a) Simulated Image



(b) 2MASS Image

Fig. 13.— MASSCLEAN simulated image of the young Milky Way cluster, *NGC 3603* is given in (a). The real image from 2MASS is given in (b). Both images represent a $4.4' \times 4.4'$ *J* Band Image

mag, $R_V = 3.1$, and a distance of 2 kpc (distance modulus 11.5 mag). The spatial distribution of the twin cluster is described by $r_t = 9.6'$ and $r_c = 7.01'$ for h Persei, and $r_t = 9.6'$ and $r_c = 8.86'$ for χ Persei. A Kroupa IMF has been used for both clusters, with $\alpha_1 = 0.3$, $\alpha_2 = 1.3$ and $\alpha_3 = 2.3$. A field star population has not been applied in this image, making it easier to see the extent of the two clusters in the simulation. Because we use a King model for the spatial extent, it would not be possible to use our code to model complex OB associations. However, it might be possible to construct a reasonable OB association using multiple bursts with differing radii and age such as demonstrated for h and χ Persei.

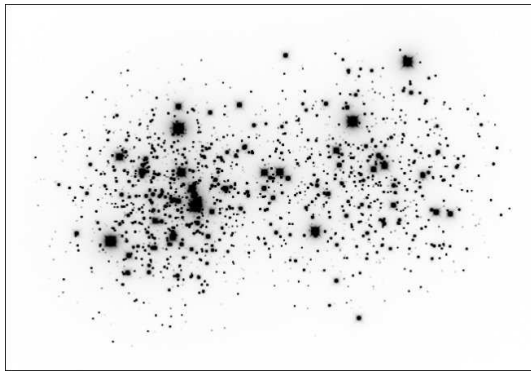


Fig. 14.— MASSCLEAN simulated image of the double Milky Way cluster, h and χ Persei (*NGC 869*, *NGC 884*). The image represents a $30' \times 30'$ field in the V band. No field star simulation is included to allow the separate cluster radii to be better viewed.

3.5. Image simulations of extragalactic clusters

Because the linear scale of the cluster (in parsecs) and distance to the cluster is determined by the user, one can use MASSCLEAN to simulate cluster at any distance, even fairly distant, barely resolved extragalactic stellar clusters. We have created a series of simulations made using the same initial inputs as in Figure 12(a) and Figure 13(a) of *Westerlund 1* and *NGC 3603*, respectively. Only now we have simulated these clusters over a range of ages $\log(\text{age}/\text{years}) = [6, 8]$ and placed the clusters at the distance of M31. The simulation is designed to represent the depth and resolution

($0.14''$) expected from the *Hubble Space Telescope* using the *Advanced Camera for Surveys* instrument. Both V-band and I-band simulated images are presented. A model for the field stars has also been applied. Our choice was to generate field stars close to the ones observed in the real images of the clusters in M31 and to keep the cluster distinguishable from the stellar field for at least 10 million years. Beside each image we provide the current view of the CMD for that cluster, all scaled to the same magnitude limits.

The images given in Figure 15, 16, 17, 18 have been created from the original MASSCLEAN generated FITS files and considerable dynamic range of the magnitudes originally contained in those FITS images have been lost. We have also been forced to select a single set of minimum and maximum brightness levels and slope to view the clusters over a large age range to show the relative change in the cluster's appearance with age. This has lead to highly degraded images. One can recover the full dynamic range of the magnitudes used by viewing the FITS files included in the electronic, on-line version of the paper.

We choose a static model for the spatial distribution in order to allow the viewer to easily compare the brightness of stars at different ages (keeping them in the same location). Naturally, clusters are prone to many kinematic disruptions, internal and external. Kinematics and disruption mechanisms could be included in a future version of MASSCLEAN since the individual stellar masses are tracked with time.

4. Applications of MASSCLEAN

MASSCLEAN is not meant to replace previous, widely used SSP models. In fact, in applications where spatial resolution is not available and spectral information is, MASSCLEAN will be an inferior choice. However, we have identified a few astronomical questions of interest to us which drove us to create an image simulation routine, based on the tenants of the modern SSP models. We will discuss just a few of these below.

4.1. MASSCLEAN as part of a Monte Carlo analysis

MASSCLEAN determines integrated luminosities and colors, such as those shown in Figure 5, based

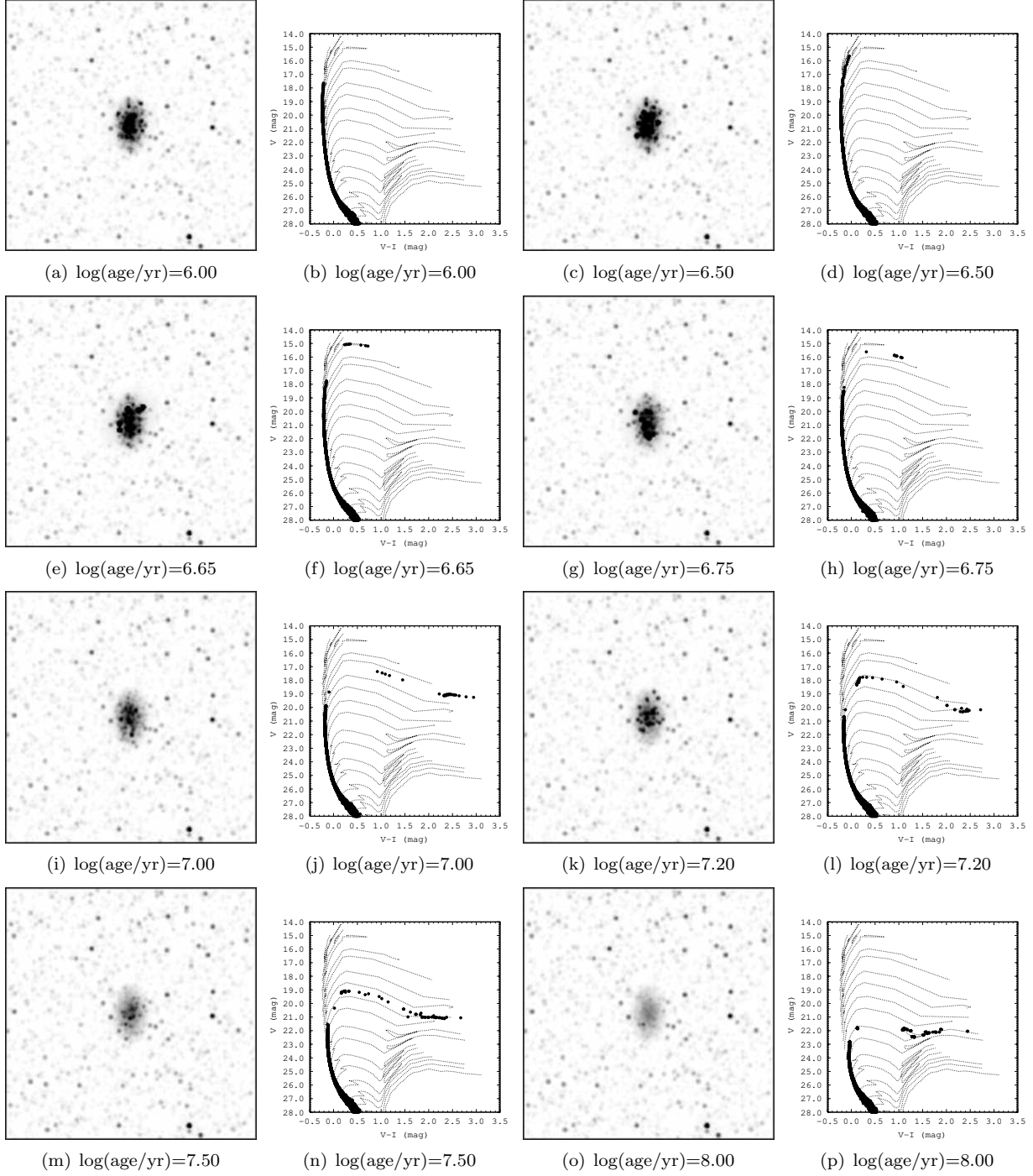


Fig. 15.— *Westerlund 1* in M31 (V Band), simulated images and color-magnitude diagrams.

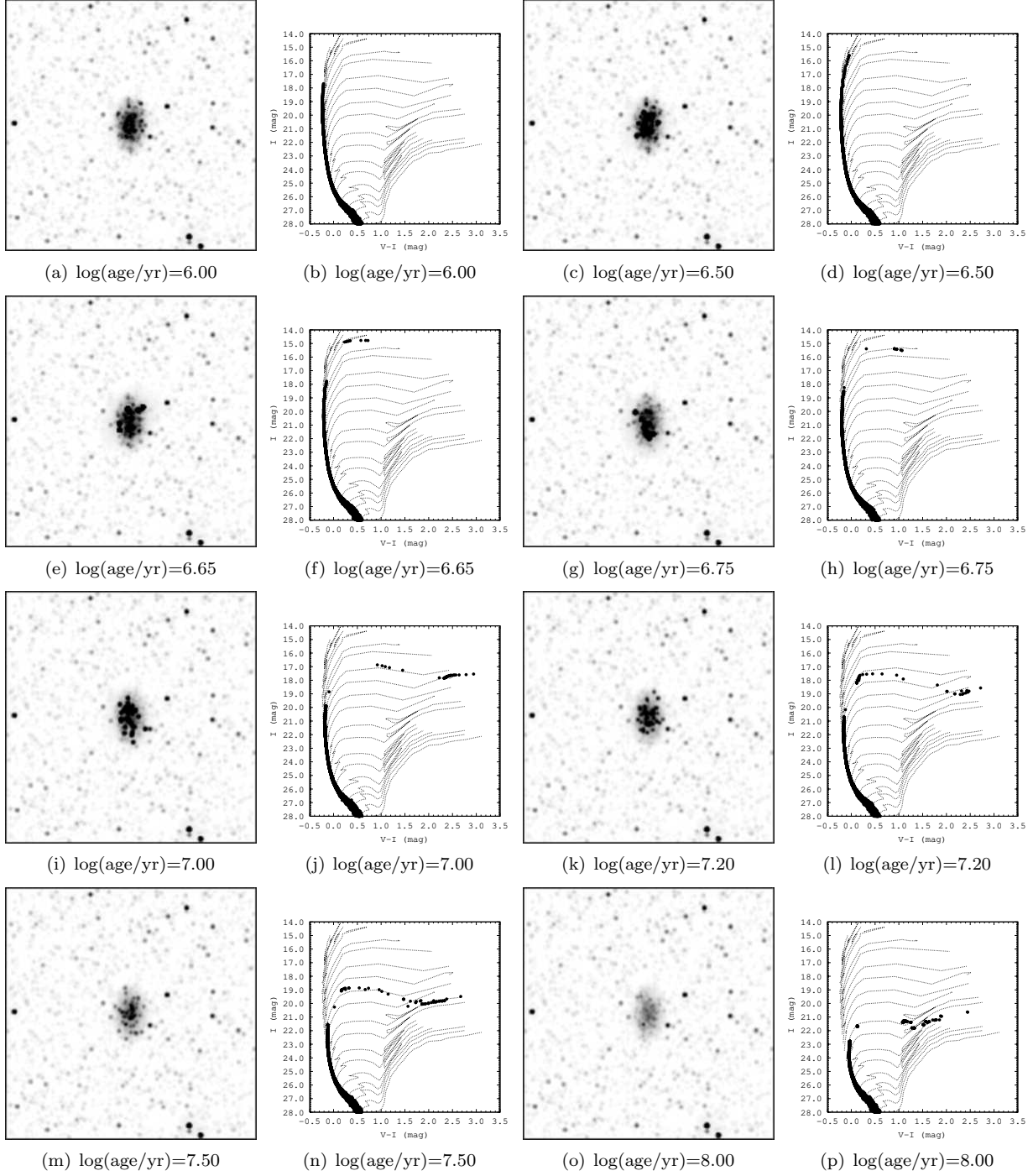


Fig. 16.— *Westerlund 1* in M31 (I Band), simulated images and color-magnitude diagrams.

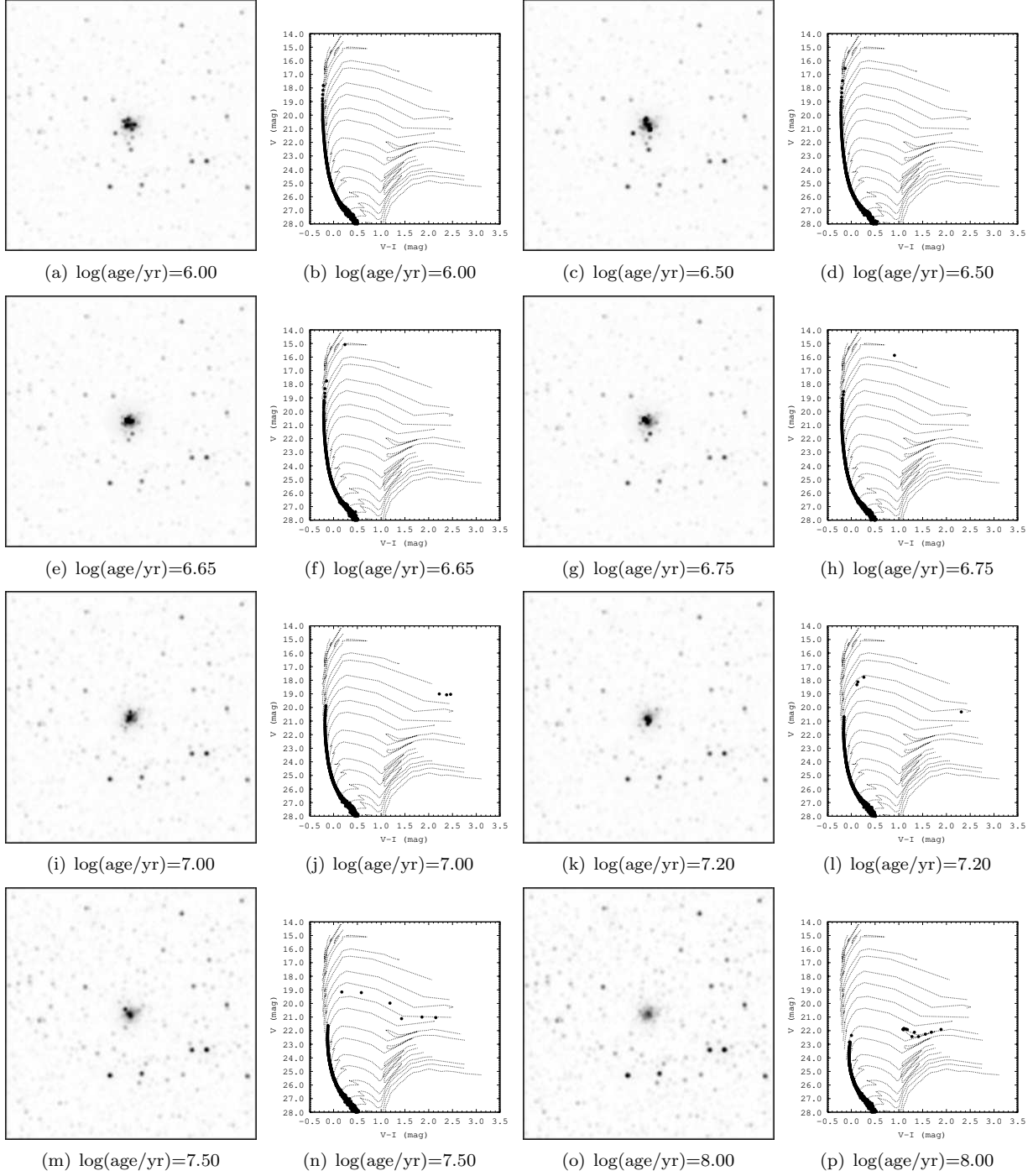


Fig. 17.— *NGC 3603* in M31 (V Band), simulated images and color-magnitude diagrams.

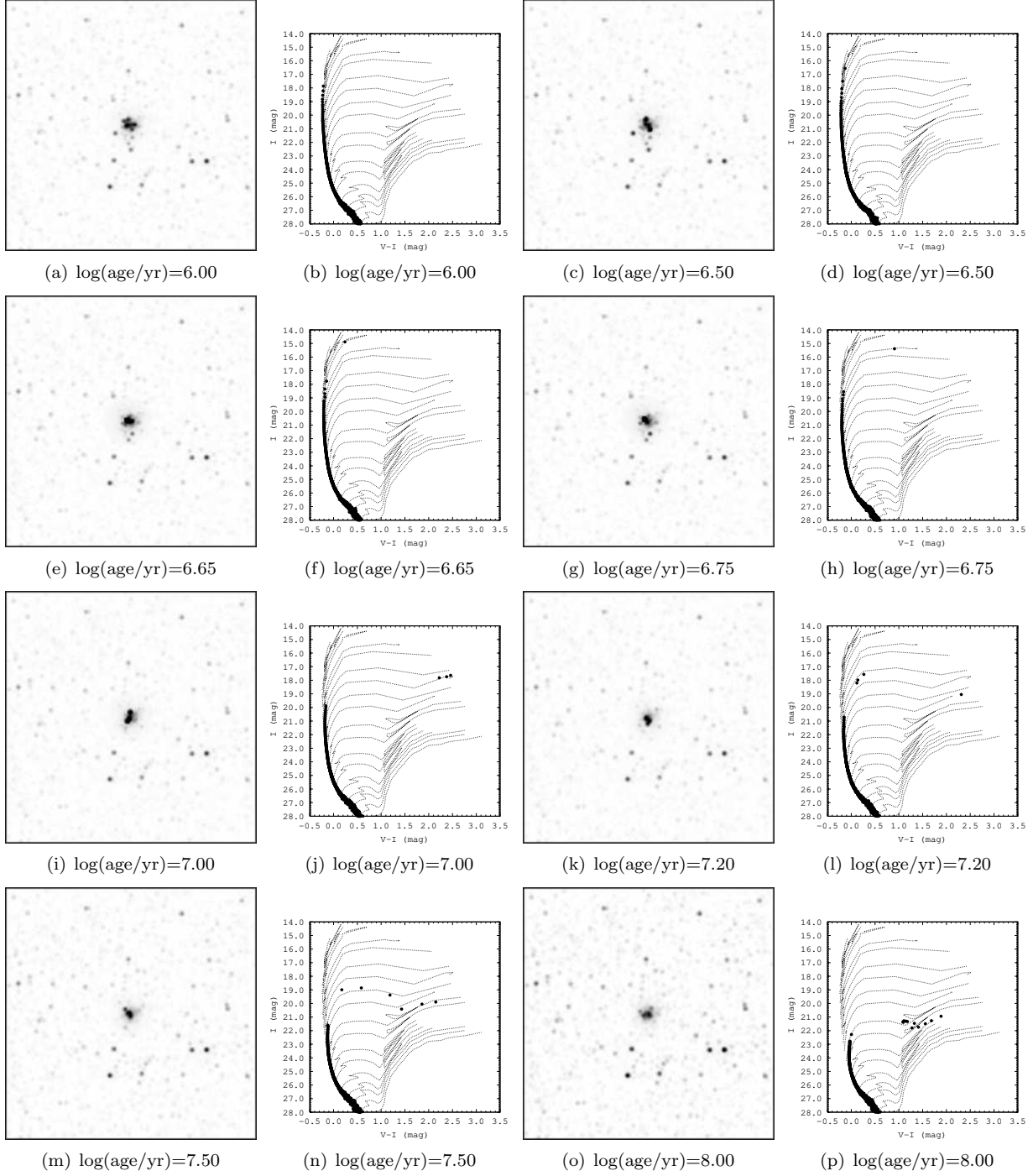


Fig. 18.— *NGC 3603* in M31 (I Band), simulated images and color-magnitude diagrams.

on the pure summing up of the luminosity of the individual objects in the simulation as individual objects are being tracked in the simulation. This is quite different from the standard SSP codes which rely on a probabilistic mass function of stars to describe luminosities (Cerviño & Luridiana 2006). In the later method, there is no way to estimate the 'stochastic fluctuations' expected with a finite number of stars in a real cluster and the range of observed integrated colors which will naturally result. The mean values derived from probabilistic models are correct on average, but they may not represent the actual values observed, particularly clusters which lie below the Lowest Luminosity Limit as described by Cerviño & Luridiana 2004. **MASSCLEAN**, when used as part of a Monte Carlo analysis, can be used to characterize the distribution of integrated properties as a function of cluster mass.

4.2. Selection effects in stellar cluster searches

Researchers have been developing systematic surveys of large scale Galactic databases in the infrared to identify new, previously unknown clusters. Some of the earliest and most successful of those were completed using the 2MASS (Skrutskie et al. 2006) survey, first and most extensively by Dutra et al. 2003 and Bica et al. 2003 and more recently by Froebrich et al. 2007. The Spitzer Space Telescope GLIMPSE galactic plane survey (Benjamin et al. 2003) and UKIDSS Galactic plane survey (Lucas et al. 2007) have recently gone public leading to additional candidate stellar cluster detections (Mercer et al. 2005).

In uncovering the galactic open and globular cluster population, researchers have become well aware of the problem of false positives. A sight-line with slightly reduced average extinction will peer deeper into the inner galaxy causing an observed stellar density enhancement, mimicking a cluster (Cotera & Leistra 2003, Froebrich et al. 2007). But false positives are not the only errors important in obtaining a complete picture of the massive star clusters of our and external galaxies. There also lies the error of the second kind: the false negative.

It has been proposed that very massive clusters do not exist in the Milky Way Galaxy, either because the Milky Way is not capable of cre-

ating very massive clusters or the power law of the cluster mass function turns over (Gieles et al. 2006a, 2006b). Since we do not see extremely massive clusters within our galaxy, do we accept that they do not exist? What if they do exist? Then we have made the error of failing to observe an object when in fact there is one. Such an error is called a false negative. The extent of false negatives is impossible to derive directly from the clusters which are detected nor analytically. An image simulation package such as **MASSCLEAN**, when used with a realistic simulation for the structure and extinction for the plane of the Milky Way, can be used to derive selection effects and expected yields from the present search methods.

4.3. Constraining field-star contamination

Beyond false negatives, efforts to identify and characterize even optically observed galactic clusters can suffer greatly from field star contamination (Bonatto et al. 2006), particularly for low-contrast clusters. Bonatto & Bica 2007 estimate that 10-20 percent of radii of open clusters may be underestimated due to the confusion brought on by high field star densities. Moreover, with time the dynamical evolution of these clusters, leading to increased mass segregation, further reduces the surface brightness at large radii. Imaging simulations can begin to address the extent of these biases in various fields, in different bands and as a function of galactic latitude, stellar field properties and cluster mass segregation.

5. Conclusion

Our **MASSCLEAN** package has been introduced. We provide a few first order checks that our simulations are consistent with other, well accepted, modern SSP codes. We have demonstrated its features simulating various clusters over a mass range of a few $\times 10^3 - 10^5 M_\odot$ and showing simulated CMDs and single-band images. Although the package can simulate low mass clusters, we emphasize its use for massive clusters due to the difficulty of such a simulation. In order to determine the mass, age and distance of a cluster, observational astronomers typically rely on the brightest stars, perhaps no more than 10% of the cluster, particularly when extinction is high. Our approach complements this effort by simulating all

of the stars (not only the visible ones). In a forthcoming paper, we will develop and present methods to derive the goodness of fit for a simulated versus a real cluster using cumulative distribution functions.

We are grateful to suggestions made to an early draft of this work by Rupali Chandar, Bruce Elmegreen, Deidre Hunter and Brad Whitmore. Their ideas lead to significant improvements in the presentation. This material is based upon work supported by the National Science Foundation under Grant No. 0607497 to the University of Cincinnati. BP was supported by a graduate summer fellowship from the University of Cincinnati's Research Council.

REFERENCES

- Anders, P. & Fritze -v. Alvensleben, U. 2003, A&A, 401, 1063
- Bahcall, J. N., Soneira, R. M. 1984, ApJS, 55, 67
- Beasley, M. A., Hoyle, F., Sharples, R. M. 2002, MNRAS, 336, 168
- Bertin, E. 2001, SKYMAKER,
<http://terapix.iap.fr/cpltd/oldSite/soft/skymaker/>
- Bertin, E. & Fouqué, P. 2007, SKYMAKER,
http://terapix.iap.fr/rubrique.php?id_rubrique=221
- Bertin, E. & Arnouts, S. 1996, A&AS, 117, 393
- Benjamin, R. A. et al. 2003, PASP, 115, 953
- Bica, E., Dutra, C. M., Soares, J., Barbuy, B. 2003, A&A, 404, 223
- Bonatto, C., Kerber, L. O., Bica, E., Santiago, B. X. 2006, A&A446, 121
- Bonatto, C. & Bica, E. 2007, MNRAS, 377, 1301
- Bragg, A.E. 2004, PhD thesis, Harvard Univ.
- Brandner, W., Clark, J. S., Stolte, A., Waters, R., Negueruela, I., Goodwin, S.P. 2008, A&A, 478, 137
- Brocato, E., Matteucci, F., Mazzitelli, I., Tornambe, A. ApJ, 349, 458
- Bruzual, G. & Charlot, S. 2003, MNRAS, 344, 1000
- Cardelli, J. A., Clayton, G. C., Mathis, J. S. 1989, ApJ, 345, 245
- Cerviño, M. & Luridiana, V., 2004, A&A, 413, 145
- Cerviño, M. & Luridiana, V., 2006, A&A, 451, 475
- Charbonnel, C., Meynet, G., Maeder, A., Schaller, G., Schaerer, D. 1993, A&A, 101, 415
- Charbonnel, C., Meynet, G., Maeder, A., Schaerer, D. 1996, A&A, 115, 339
- Charbonnel, C., Däppen, W., Schaerer, D., Bernasconi, P. A., Maeder, A., Meynet, G., Mowlavi, N. 1999, A&A, 135, 405
- Charlot, S., Bruzual, G. A. 1991, ApJ, 367, 126
- Charlot, S. 1996, in ASP Conf. Ser. 98, From Stars to Galaxies: The Impact of Stellar Physics on Galaxy Evolution, ed. C. Leitherer, U. Fritze von Alvensleben, & J. Huchra (San Francisco: ASP), 275
- Clark, J. S. & Negueruela, I. 2002, A&A, 396, L25
- Clark, J. S., Negueruela, I., Crowther, P. A., Goodwin, S. P. 2005, A&A, 434, 949
- Cohen, M. 1994, AJ, 107, 582
- Cohen, M. 1995, ApJ, 444, 874
- Cotera, A. & Leistra, A. 2003, BAAS, 35, 1249
- Dutra, C. M., Bica, E., Soares, J., Barbuy, B. 2003, A&A, 400, 533
- Figer, D. F., MacKenty, J. W., Robberto, M., Smith, K., Najarro, F., Kudritzki, R. P., Herrero, A. 2006, ApJ, 643, 1166
- Froebrich, D., Scholz, A., Raftery, C. L. 2007, MNRAS, 374, 399
- Fusi Becci, F., Bellazzini, M., Buzzoni, A., De Simone, E., Federici, L., Galletti, S. 2005, AJ, 130, 554
- Gieles, M., Larsen, S. S., Scheepmaer, R. A., Bastian, N., Haas, M. R., Lamers, H.J.G.L.M. 2006a, A&A, 446, 9
- Gieles, M., Larsen, S. S., Bastian, N., Stein, I. T. 2006b, A&A, 450, 129
- Girardi, L., Chiosi, C., Bertelli, G., Bressan, A. 1995, A&A, 298, 87
- Holtzman, J. A., et al. 1992, AJ, 103, 691
- Hurley, J. R., Pols, O. R., Tout, C. A. 2000, MNRAS, 315, 543

- King, I. 1962, *AJ*, 67, 471
- Kroupa, P. 2002, *Sci*, 295, 82
- Leitherer, C., et al. 1999, *ApJS*, 123, 3
- Lejeune, T., Cuisinier, F., Buser, R. 1998, *A&AS*, 130, 65
- Lejeune, T. & Schaerer, D. 2001, *A&A*, 366, 538
- Lucas, P. W., et al. 2008, *MNRAS*, 391, 136
- Maraston, C. 2005, *MNRAS*, 362, 799
- Marigo, P., Girardi, L., Bressan, A., Groenewegen, M. A. T., Silva, L., Granato, G. L. 2008, *A&A*, 482, 833
- Mercer, E. et al. 2005, *ApJ*, 635, 560
- Meynet, G., Maeder, A., Schaller, G., Schaerer, D., Charbonnel, C. 1994, *A&AS*, 103, 97
- Mowlavi, N., Schaerer, D., Meynet, G., Bernasconi, P. A., Charbonnel, C., Maeder, A. 1998, *A&AS*, 128, 471
- Oey, M. S. & Clarke, C. J. 2005, *ApJ*, 620, L43
- Pessev, P. M., Goudfrooij, P., Puzia, T. H., Chandar, R. 2008, *MNRAS*, 385, 1535
- Salpeter, E. E. 1955, *ApJ*, 121, 161S
- Schaerer, D., Charbonnel, C., Meynet, G., Maeder, A., Schaller, G. 1993, *A&AS*, 102, 339
- Schaerer, D., Meynet, G., Maeder, A., Schaller, G. 1993, *A&AS*, 98, 523
- Schaller, G., Schaerer, D., Meynet, G., Maeder, A. 1992, *A&AS*, 96, 269
- Schulz, J., Fritze – v. Alvensleben, U., Möller, C. S. Fricke, K. J. 2002, *A&A*, 392, 1
- Skrutskie, M. F., et al. 2006, *AJ*, 131, 1163.
- Stolte, A., Brandner, W., Brandl, B., Zinnecker, H., Grebel, E. K. 2004, *AJ*, 128, 765
- Stolte, A., Brandner, W., Brandl, B., Zinnecker, H. 2006, *AJ*, 132, 253
- Tinsley, B. M. & Gunn, J. E. 1976, *ApJ*, 203, 52
- Tinsley, B. M. 1978, *ApJ*, 222, 14
- Vazquez, G. A., Leitherer, C. 2005, *ApJ*, 621, 695
- Wainscoat, R. J., Cohen, M., Volk, K., Walker, H. J., Schwartz, D. E. 1992, *ApJS*, 83, 111
- Westerlund, B. 1961, *PASP*, 73, 51
- Whitmore, B. C. & Schweizer, F. 1995, *AJ*, 109, 960
- Zacharias, N., Monet, D. G., Levine, S. E., Urban, S. E., Gaume, R., Wycoff, G. L. 2004, *AAS*, 205, 4815